SEMARAK ILMU PUBLISHING

Journal of Advanced Research in Fluid Mechanics and Thermal Sciences

Journal homepage:
https://semarakilmu.com.my/journals/index.php/fluid_mechanics_thermal_sciences/index
ISSN: 2289-7879

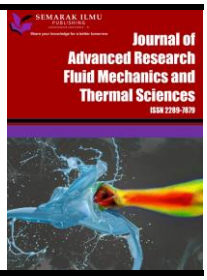

The Influence of Different Mass Ratios on Vortex-Induced Vibration Energy Extraction of Four Cylinder Arrays

Fatin Alias[1], Mohd Hairil Mohd[1], Mohd Asamudin A. Rahman[1,*]

[1] Maritime Technology & Naval Architecture Programme, Faculty of Ocean Engineering Technology, Universiti Malaysia Terengganu, 21030 Kuala Nerus, Terengganu, Malaysia

ARTICLE INFO

Article history:
Received 24 November 2023
Received in revised form 20 April 2024
Accepted 2 May 2024
Available online 30 May 2024

Keywords:
Vortex-induced vibration; energy harvesting; mass ratio; marine energy

ABSTRACT

Currently, there is a growing demand for renewable energy harnessed from fluid dynamics within the oil and gas industry. The surge in demand has propelled electricity to become a vital and irreplaceable form of universal energy worldwide. Vortex-Induced Vibrations (VIV) energy harvesting shows great potential as a technology for capturing energy from flowing bodies of water. The purpose of this research is to investigate the numerical aspect of VIV in rigid circular cylinders with the intention of capturing renewable energy from the sea. The investigation employs a Vortex-Induced Vibration Aquatic Clean Energy (VIVACE) converter to analyze the vibration characteristics of densely packed cylinders featuring varying mass ratios (m*) at both minimum and maximum values. Another purpose of the study is to investigate the effect that m* has on the performance of a VIV converter that is comprised of four cylinders positioned in a staggered pattern. For the purpose of analyzing power conversion in the VIV energy converter model across a wide range of mass ratios (from 2.36 to 12.96), simulations are carried out with a Reynolds number of 82000. The findings indicate that the highest converted power reaches a peak of 7.48 W with a mass ratio of 2.36, whereas a greater mass ratio of 12.96 results in only 4.33. The study highlights the substantial influence of mass ratios on the extraction of power output from VIV. The results essentially offer crucial information about the optimum mass ratio in closed four cylinder arrays to design VIV energy harvesting to produce clean and renewable energy sources.

1. Introduction

Vortex-Induced Vibrations (VIV) are of significant relevance in the offshore sector. The vibrations are observed in the form of hydrodynamic forces, which generate vortices that interact with pliable structures. The observed phenomena of nonlinear flow structure arise from this interaction, and it has significant significance in multiple engineering disciplines, including subsea, civil, aeronautical, oceanographic, and mechanical [1]. A significant amount of studies have been dedicated to understanding the intricacies of VIV, including a wide range of numerical and experimental studies as well as extensive review publications [2-5]. Numerous issues raised by VIV have been the driving

* *Corresponding author.*
E-mail address: mohdasamudin@umt.edu.my

https://doi.org/10.37934/arfmts.117.2.114

force for a significant amount of investigation in the field. The effects of VIV are far-reaching and have an immense effect on the design and operation of offshore constructions as well as other fluid systems. In order to get a more in-depth understanding of VIV, recent attempts have made use of analyses, numerical simulations, and experiments. Some of the researchers who contributed to this study are Gonçalves *et al.,* [3], Han *et al.,* [4], Wang and Zhao [6] and also Williamson and Govardhan [7], and these are only a few of them. VIV may be generated by two distinct forms of oscillations: self-excited oscillations and forced oscillations, which are alternatively known as vibration-induced vortices. Furthermore, VIV may occur either spontaneously or as a result of involuntary oscillations at different speeds and magnitudes [8-10]. The research conducted by Min *et al.,* [10] showed that a Reynolds number of 80 successfully mitigated the wake, hence facilitating the positioning of a compact control cylinder downstream of the primary cylinder within close proximity of the wake [11].

Instead of attempting to dampen the vibrations, the VIV will be transformed into a source of energy that may be put to good use [12]. As a result, the engineering industry came up with a mechanism to solve the issue and make use of the vast quantities of renewable electricity that are accessible in the marine environment and other forms of water [13]. One of the most difficult challenges in the current economic climate and a potentially severe scenario for the natural gas and oil sector is to ensure that the industry has sufficient energy to support its economic expansion while simultaneously reducing its effect on the environment. One of the devices that Bernitsas *et al.,* [14] developed is called the VIVACE converter. This device was developed on the basis of optimizing vortex shedding rather than removing it. A VIVACE converter is able to transform the energy of the ocean into electrical energy. Energy can be generated by a variety of sources, including wind, tidal, solar, ocean waves, and mechanical vibrations, among others. The VIVACE converter type has a notable capacity for producing a high-power conversion ratio, enabling it to create energy even when subjected to currents as low as 0.25m/s. This specific ability facilitates the extraction of significant amounts of energy from ocean and river currents, hence increasing their economic effectiveness. In order to establish a high-power configuration for the VIVACE converter array, as seen in Figure 1, it is necessary to link many converters.

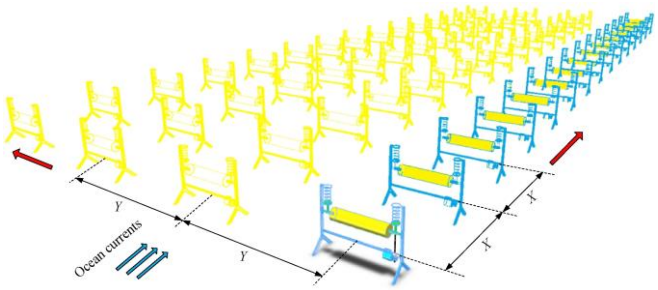

Fig. 1. A schematic of VIV power generation [15]

Besides, the study of VIV for energy harvesting has been the subject of extensive research, particularly concerning the influence of m* on amplitude and frequency responses. The m* has been highlighted as a crucial role in these responses. Fredsoe and Sumer [16] further elaborated on this, emphasizing that a lower m* tends to result in higher amplitudes and frequencies in the VIV phenomenon. They also noted that the specific m* utilized in previous studies varied depending on the fluid medium. For instance, in air, a high m* ranging from 100 to 1000 was typically employed, while in water, a lower m* ranging from 1 to 10 was more common. This understanding underscores the importance of considering the fluid medium when determining the effect of m* on VIV.

Recent research has delved into specific scenarios of VIV involving cylinders with varying m*. Reyes and Mandujano [17] investigated the VIV of a cylinder at low m*, exploring the dynamics under

different conditions. Gonçalves *et al.,* [18] contributed to this area by studying two degrees of freedom VIV of circular cylinders with small m*. They found that as the m* decreased, the amplitude increased, with specific values recorded for different configurations. Additionally, Liu *et al.,* [19], conducted a numerical investigation focusing on m* less than 1.0. Their study provided insights into the behavior of VIV for low m* under specific conditions, such as Reynolds number and damping ratio. These studies collectively contribute to the understanding of how m* impacts VIV phenomena in varying conditions and configurations.

According to Zahari and Dol [20], the electricity that is created from the water current not only originates from a source that is both renewable and environmentally friendly but also gives precedence to the preservation of the environment when it comes to delivering power to the offshore station. The increased demand that occurs during maintenance activities causes the power consumption on the offshore platform to be much greater. Therefore, for the platform to function continuously, it is necessary to have electrical services that are both consistent and reliable. This is especially important for independent platforms that rely significantly on machines to function.

This study aims to explore the impact of mass ratio on vibration synchronization in a model of VIV energy extraction. It employs Computational Fluid Dynamics (CFD) methods to analyze the harvested energy from VIV across four cylinders with different mass ratios. The research demonstrates the effectiveness of utilizing multiple cylinders compared to a single cylinder in power generation. Notably, the configuration of four staggered cylinders with varying mass ratios show significant influence on energy harvesting due to differences in wake energy.

2. Methodology

2.1 Governing Equations

In a fluid channel, simulations were conducted on the flow of an unsteady, Newtonian, and incompressible fluid past a cylinder. The equations that regulate fluid motion are referred to as the Navier-Stokes equation.

2.1.1 Continuity equations

The continuity equation, often referred to as the instant mass conservation equation, is formulated by applying the principle of mass conservation to a specific fluid volume in the case of a general fluid, as shown in Eq. (1) [21].

Its differential form is written as

$$\frac{\partial \rho}{\partial t} + \nabla . (\rho \, \vec{u}) = 0 \tag{1}$$

where,
ρ is the fluid density
t is time
$\vec{u}$ is the flow velocity vector

The first term $\frac{\partial \rho}{\partial t}$ denotes the rate of change of density in regard to time. Meanwhile, the second term $\nabla . (\rho \, \vec{u})$ express the divergence of the vector field $\rho \, \vec{u}$ at a specific point fixed in space. Eq. (2)

provides an expression for the continuity equation that can also be represented through the use of the substantial derivative [21]

$$\frac{D\rho}{Dt} + \nabla . (\rho\, \vec{u}) = 0 \tag{2}$$

2.1.2 Momentum equations

The conservation equation for momentum is established by applying Newton's second law of motion to the fluid control volume, where the rate of change of fluid particle momentum equals the combined surface and body forces. This law applies because the fluid control volume is a form of liquid. It is specified in Eq. (3) that the momentum equation is as follows [22]

$$\rho \frac{\partial \vec{u}}{\partial t} + \ (\rho\, \vec{u} \ \cdot \ \nabla) = 0 - \nabla \mathrm{p} + \rho \mathrm{b} + \nabla \cdot \tau \tag{3}$$

where,
p is the pressure
b is the source term (generally gravity)
τ is the viscous stress tensor

In the case when the fluid is Newtonian, the viscous stresses are directly proportional to the rate at which strain will occur over time. The stress tensor in Eq. (4) is simplified by the Stokes hypothesis when applied to a Newtonian fluid [22]

$$\tau_{ij} = \mu(\frac{\partial u_i}{\partial x_j} + \frac{\partial u_j}{\partial u_i}) - \frac{2}{3}\mu\delta_{ij}\frac{\partial u_k}{\partial u_k} \tag{4}$$

where μ is the dynamic viscosity of the fluid.

Following the completion of several validation procedures, the turbulence model of k-ω was utilized for the simulation in the CFD study. This was done in accordance with the various types of flow and the required degree of accuracy in the turbulent flow simulation, which was performed on the background velocity profile and wake.

2.2 Geometrical Modelling and Boundary Condition

Figure 2 presents four different cylinders that were used in this investigation. These cylinders were identified as C-P, C-Q, C-R, and C-S. On both sides of C-P and C-Q, C-R and C-S are positioned in a symmetrical position and are slightly staggered from one another. The simulation was then performed based on a single degree of freedom (SDOF). The damping constant, denoted by c, and the spring damper, denoted by k, make up the elastic system. The values of the physical parameters that were utilized in the current model are reported in Table 1. It is important to note that the simulation utilized the Reynold Number, which is equal to 8.2×10^4. This particular value corresponds to the turbulent flow regime because the condition of the wake is absolutely turbulent [23].

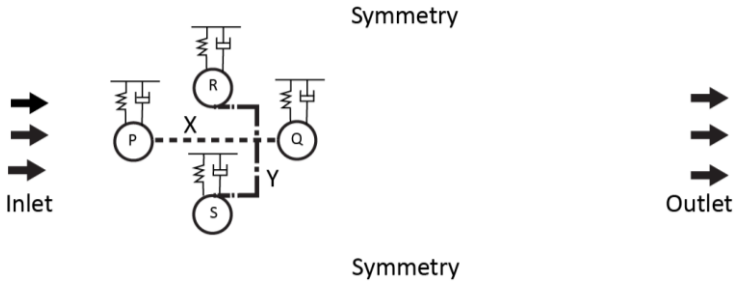

Fig. 2. Schematic drawing of the four cylinders (not to scale)

Table 1
Physical Parameter for Present Model

Parameter	Value
Mass ratio (m*)	2.36-12.96
Diameter ratio, d/D (m)	0.09
Damping ratio (ξ_{total})	0.02
Reduced Velocity (V_r)	8
Reynolds Number (Re)	8.2×10^4
Density,ρ (kg/m^3)	1025
Kinematic viscosity, *v* (m^2/s)	1.1×10^{-6}
Spring stiffness K (N/m)	814

A Reynold Number of 82000 was found to match the mean velocity of the uniform flow inside the inlet boundary. For the model consisting of several cylinders with a variety of m*, the Reynolds number, damping ratio, and spring stiffness will all be constant variables. Also, the majority of the VIV responses are determined by the m* and lowered velocity, both of which are critical parameters. The respective definitions are described in Eq. (5) and Eq. (6).

$$m^* = \frac{4m}{\pi \rho D^2} \tag{5}$$

$$V_r = \frac{V}{D f_n} \tag{6}$$

The equation incorporates many factors, including m, which denotes mass per unit length and is associated with decreased velocity, the ratio of cylinder wavelength to diameter throughout its trajectory, and f_n, which represents the standard water frequency at which a cylinder oscillates in water [16,24,25]. In order to evaluate the energy transfer from the cylinder's flow throughout a single cycle, Eq. (7) and Eq. (8) are used.

$$E_{VIV} = \frac{1}{2} K A^2 + 2\pi^2 C_{total} f_{osc} A^2 \tag{7}$$

$$P_{VIV} = \frac{1}{T_{osc}} E_{VIV} \tag{8}$$

The flow of VIV power is assessed during each oscillation cycle, where K represents the spring stiffness, A denotes the amplitude of the waves, C_{total} is the coefficient of damping in a system, and f_{osc} expresses the cylinder's vibration frequency [25]. After that, the power-to-volume density of the VIV converter model, denoted by P_{VIV_V}, was computed using the VIV power of the stagger cylinders P_{VIV} as described in Eq. (9).

$$P_{VIV\_V} = \frac{P_{VIV}}{1 \times XY} \tag{9}$$

The boundary criteria outlining the domain are shown in Table 2, offering an in-depth perspective. Slip walls were carefully chosen so that there would be no shear stress between the fluid and the walls while modeling the pressure outlet limits. Particularly, the consideration of viscous stress at the outflow was not taken into account. Moreover, it is crucial to emphasize that the solution successfully reached stability while using a 0.05-second time step.

Table 2
The Boundary Condition of the Present Model

Type of boundary conditions	Surface Name
Wall	C-P, C-Q, C-R and C-S
Symmetry	Top, Bottom, and Sides
Inflow	Inlet
Outflow	Outlet

2.3 Mesh Independence Study

For the purpose of achieving a stable solution for the numerical models, mesh independence research was carried out. A cylinder's computational mesh configurations for the simulation domain are shown in Figure 3. At a number of elements that varied from 100,000 to 130,000, the simulations started to converge at approximately Ay/D = 0.9382, as can be observed from the diagram in Figure 4. In brief, the recorded response data of the amplitude demonstrate a satisfactory correlation.

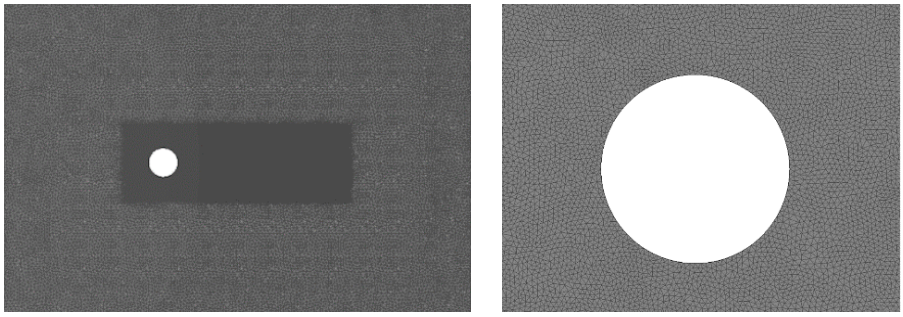

(a) (b)

Fig. 3. Computational domain meshes of a cylinder. (b) Illustration of close-up mesh

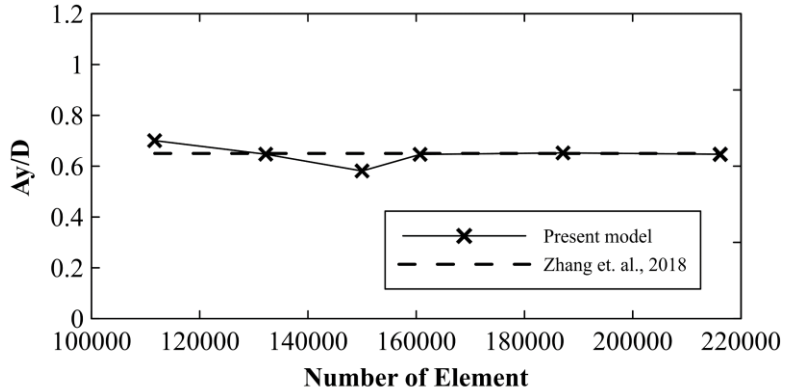

Fig. 4. Mesh Independence Study for the present model

2.4 Model Validation

The validation process is carried out in order to ascertain whether or not the computational technique used by the existing CFD model is both feasible and successful. Figure 5 presents the configuration and computational meshes of four cylinders. Validation of the current model was carried out by taking into consideration the research carried out by Zhang *et al.,* [25]. Table 3 provides a breakdown of the physical criteria that are required for the validation process. There is a significant connection between the present model and published literature, as shown in Figure 6. On the horizontal axis, the X(D) distance is plotted against the maximum amplitude, Ay/D. The error rate for validation was maintained below 5%. Based on the results of the computations, it is important to highlight that increasing the velocity results in a significant reduction in the amplitude of the cylinder.

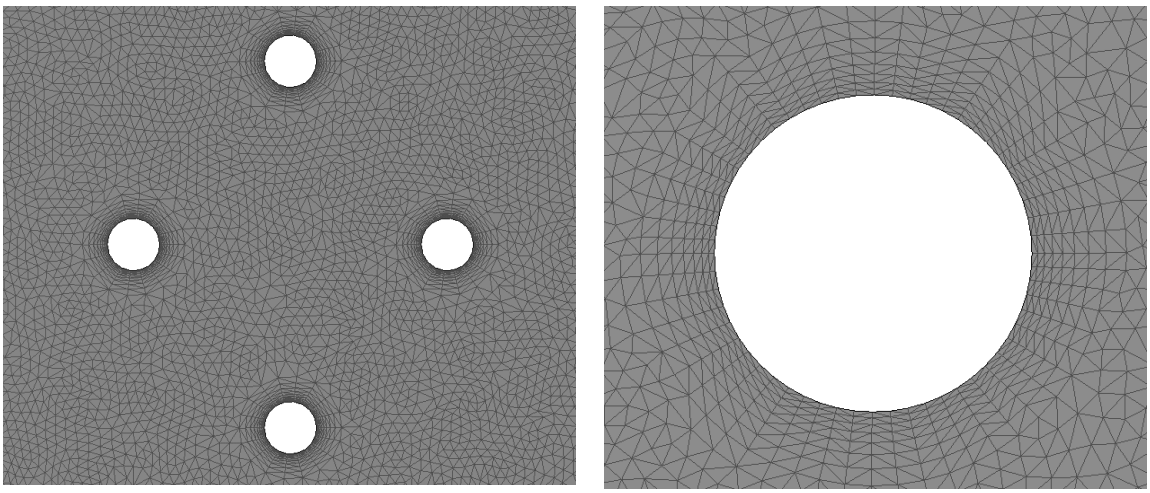

(a) (b)

Fig. 5. (a) Computational domain meshes of four cylinders, (b) Illustration of close-up mesh

Table 3
Physical Parameter for Model Validation

Parameter	Value
Mass ratio (m*)	1.36
Diameter D (m)	0.09
Damping ratio (ξ_{total})	0.02
Reduced Velocity (V_r)	8
Reynolds Number (Re)	8.2×10^4
Density ρ (kg/m³)	1025
Kinematic viscosity *v* (m^2/s)	1.1×10^{-6}
Spring stiffness K (N/m)	814
Distance X(D)	2, 4, 6 and 8
Distance Y(D)	7

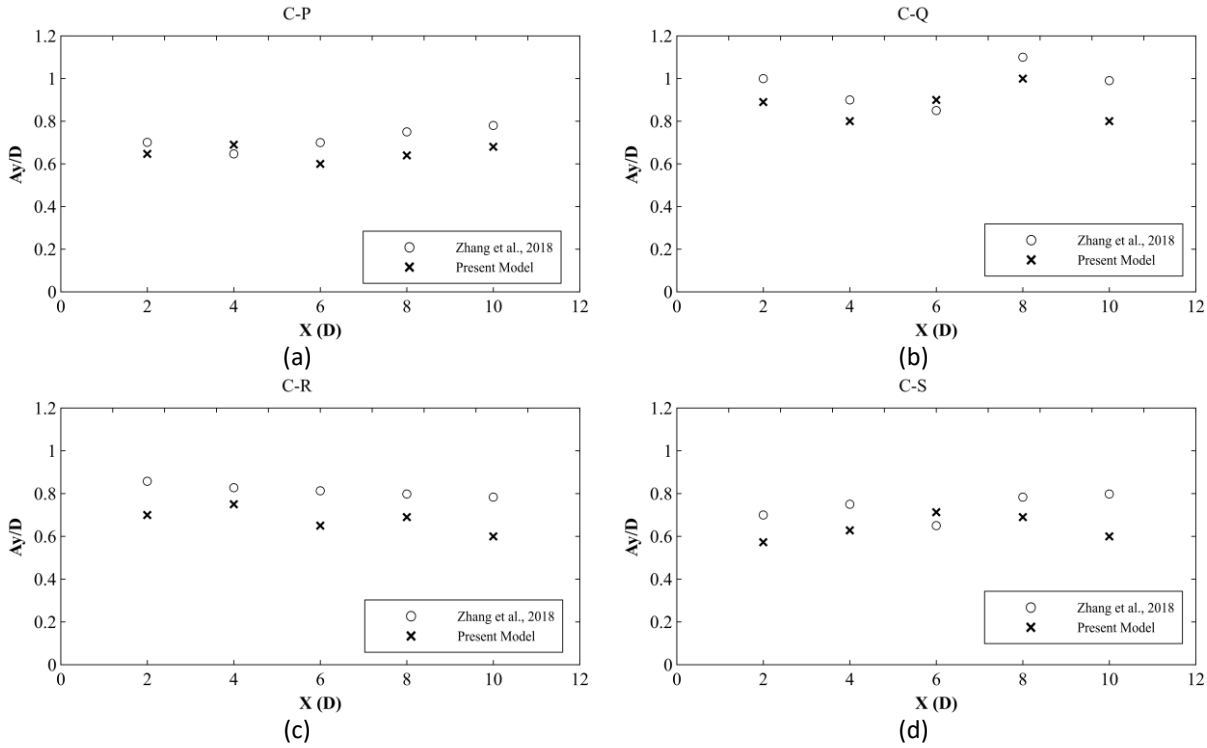

Fig. 6. Comparison and validation of the amplitude-frequency between the present model and Zhang *et al.,* [25]

3. Results

For the purpose of this investigation, four cylinders with different m* were examined. When the frequency of oscillation has reached the same level as the frequency of vortex shedding, a cylinder is considered to be "locked-in." The most significant amplitude oscillations were observed in this particular region. Figure 7 depicts the frequency response of the cylinder as a function of the decreased velocity, V_r. At the outset, there was instability or lack of synchronization between the Vortex Shedding frequency, F_{VS} and the Vibration frequency, F_V. The explanation for this is because the cylinders are vulnerable to the impact of fluid forces. It is apparent that while the reduced velocity was low, the frequencies were similarly low because the vortex shedding failed to develop completely.

At V_r= 8, the occurrence of a lock-in regime is quite evident. Here, with an increase in reduced velocity, the vibration amplitude gradually decreases. This phenomenon is attributed to the slower mean flow in the wake compared to the free stream. According to findings by Derakhshandeh and Alam [26], both the lock-in range's size and the vibration amplitude within this range are contingent upon the m*.

The lock-out region is characterized by a significant rise in frequency from V_r= 10 to V_r= 18. This surge may be due to the considerable volumes of vortices that are present in the wake during high-velocity flow. As a consequence, the frequencies for vortex shedding behind the cylinder are increased. In addition, it exhibits the largest amplitude over the entirety of the response range. In their study, Xu *et al.,* [27] proposed that the synchronization of vortex shedding was responsible for triggering significant oscillations in amplitude. The significant amplitude at extremely high reduced velocities was determined to be sustained by flow interference.

The Strouhal number (S_t) was defined as the linear relationship between the vortex shedding frequency curve and the cylinder. The examination of the graph demonstrates the presence of a

linear equation, denoted as y = 0.17x + 0.0127. As a result, the calculated value suggests that S_t is equal to 0.17, which approximately corresponds to 0.20. The impact of both the length of vortex formation and lateral diffusion of vorticity inside the shear layers on the Strouhal frequency was proven by Desai *et al.,* [28]. The researchers measured diffusion by adding a diffusion length that is linked to the thickness of the shear layer. They claimed that a longer diffusion length leads to the production of vortices, which in turn results in a lower Strouhal number. Furthermore, the authors contended that the increased duration of vortex formation enhances the importance of diffusion length since the shear layer diffuses prior to the formation of the vortex.

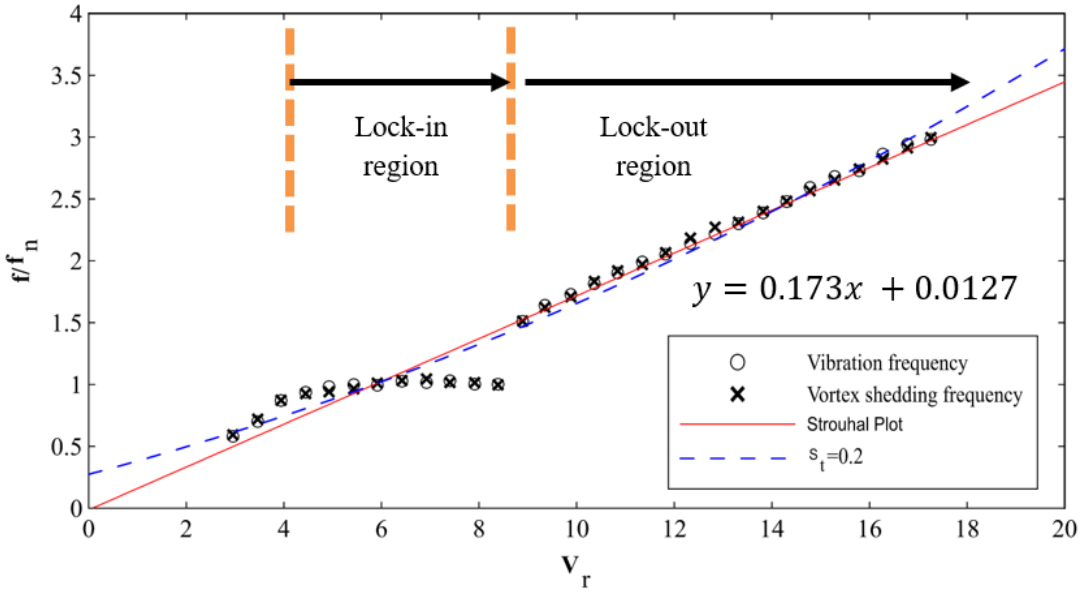

Fig. 7. Frequency ratios

The results of the amplitude ratio graph are shown in Figure 8. It is critical to highlight that the fundamental objective of this study is to investigate the influence of m*. The velocity of the lowest cylinder in the series (C-Q) is significantly impacted by the interrupted flow originating from C-P and the neighboring cylinders, C-R and C-S, particularly when the cylinders are in close proximity (see Figure 9). The analysis of VIV responses in cylinders with high and low m* demonstrates significant disparities that may be attributable to changes in m* [29]. Numerical simulations are conducted to extensively investigate the influence of various m* on the vibrations of the four cylinders inside the VIV waves. The simulations include a range of m* from 2.36 to 12.96. It is evident from the observation of C-Q that lower m* provides greater amplitudes than larger m*. It should be noted that the frequency of vibrations rises as the velocity of the flow increases. Moreover, when integrating experimental findings, it becomes apparent that numerical amplitudes exhibit a comparable pattern to power conversion. The distinct power levels generated by lock-in and lock-out reactions are contingent upon the differentiation of decreased velocity and m* ranges.

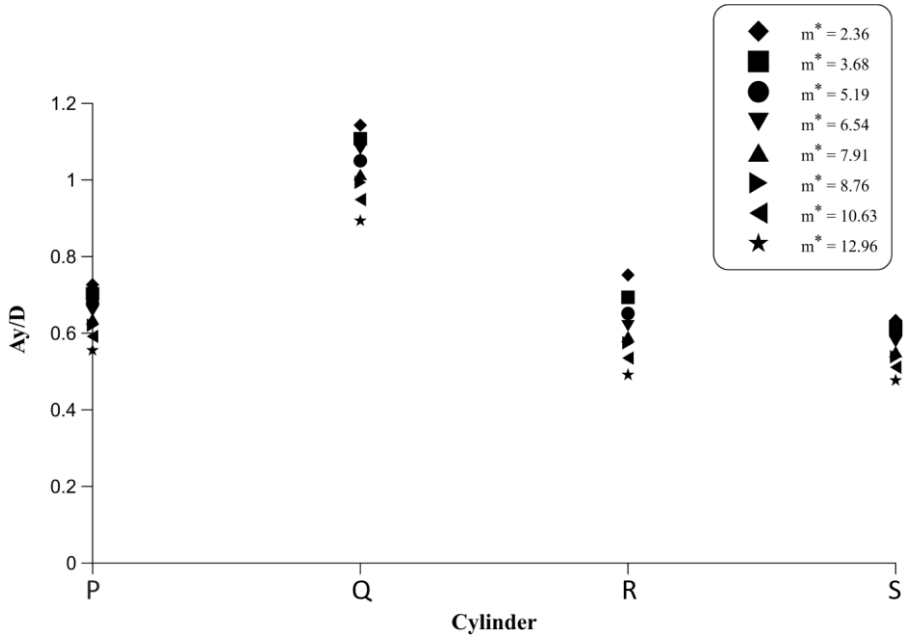

Fig. 8. Amplitude Ratio for the four cylinders with different m*

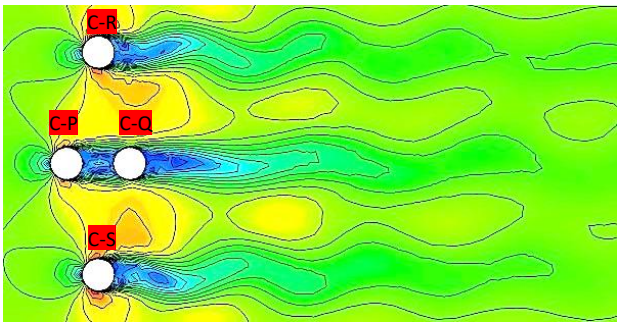

Fig. 9. Vorticity contour of four cylinders

The converted power P_{VIV} for each of the four cylinders with different m* is shown in Figure 10, offering a more transparent representation of the link between power and m*. Deformations occur as a consequence of the close proximity of cylinders during the process of power conversion. This study investigates the comparison of converted power between low and high m*. Considering that power is a measure of the energy consumption rate (calculated by dividing energy by time), the amount of energy may be determined by multiplying the power unit by the time unit. By functioning in a manner similar to that of a generator, the power converter, which is an integrated electrical device, is able to successfully harness the energy that is collected inside the VIVACE system in order to create electrical power.

As shown in the prior discussion, the cylinder located upstream (C-P) encounters low vibration as a result of obstruction caused by the cylinder located downstream (C-Q). A drop in the m* leads to a rise in both amplitude and power production, whereas an increase in the m* is associated with a decrease in power generation. The power curve for C-P exhibits a peak of 2.8 W when the highest converted power gathered from VIV responses is m* = 2.36. In contrast, the power curve has a minimum converted power of 1.61 W at m* = 12.96.

A noticeable gap is seen when comparing the m* of C-Q with those of other cylinders. Obstruction from C-Q causes flow disturbance in C-P, resulting in a substantial rise in amplitude in C-Q. The increased speed of the cylinder downstream, caused by the energy generated by the wake and the effects of contact, highlights the area with a high amount of energy. The maximal power conversion

reaches its highest at 7.48 W when m* is equal to 2.36. Nevertheless, it is worth noting that a high m* significantly lowers the energy conversion curve.

The greatest converted power achieved by C-R is 2.99 W, whilst C-S achieves a maximum of 2.14 W. In contrast, it can be seen that the minimal power production for C-R is 1.28 W, whereas C-S generates a mere 1.2 W at m* = 12.96. The analysis of power conversion curves reveals that the strategic arrangement of cylinders facilitates enhanced energy extraction from high to low m*. It is evident that the configuration of the four closely spaced cylinders maximizes the power-to-volume ratio.

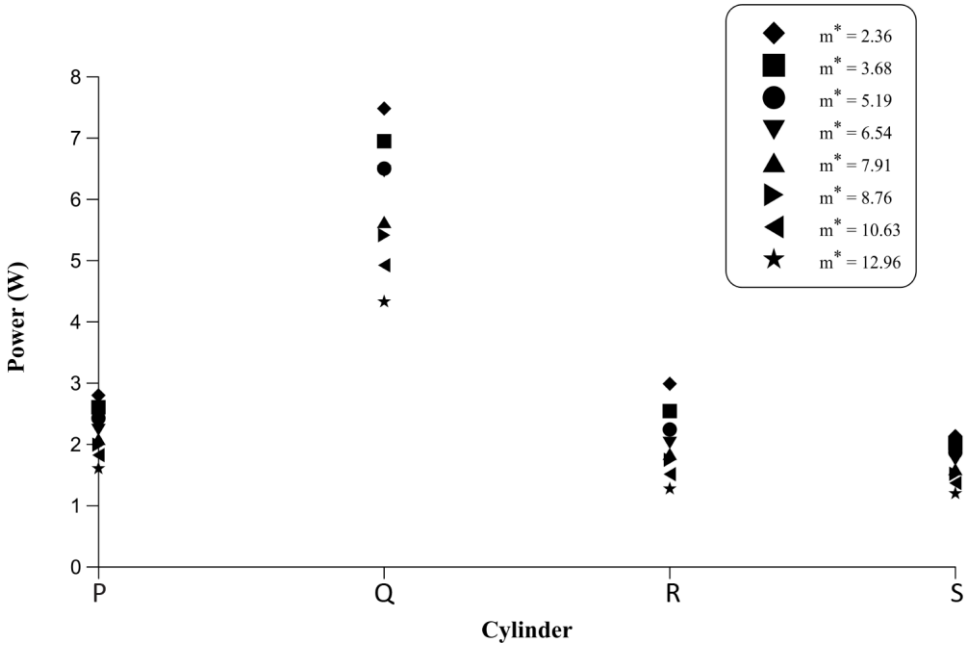

Fig. 10. Maximum Power and Energy Conversion for the four cylinders with different m*

The parameter identified as P_{VIV_V} represents the power-to-volume density, which quantifies the energy conversion capability of a cylinder in relation to the volume of ocean current it catches. Figure 11 displays a graph illustrating the power produced per unit volume (per 1 m^3 of water), denoted as P_{VIV_V}. This research examines the power stored in a system of space per unit volume. Although the power generated by a single converter may not be significant, comparing it to a single cylinder for a generator might uncover notable differences in power production.

The power-to-volume density curve exhibits alignment with both the amplitude ratio curve and the converted power curve. According to the graph, it can be seen that the four cylinders exhibit a greater power-to-volume density when their m* is lower, resulting in an increase in velocity reduction. As the m* decreases, the power-to-volume density increases, leading to greater densities for C-P, C-R, and C-S.

The alignment of the observation with converted power indicates that C-Q is the leading power generator. This may be attributed to the increased vibration caused by vortex flow originating from C-P, resulting in a higher power-to-volume density. When the m* of m* is low, specifically at m* = 2.36, the power-to-volume density exhibits a maximum value of 65.99 W/m^3 and a lowest value of 18.85 W/m^3.

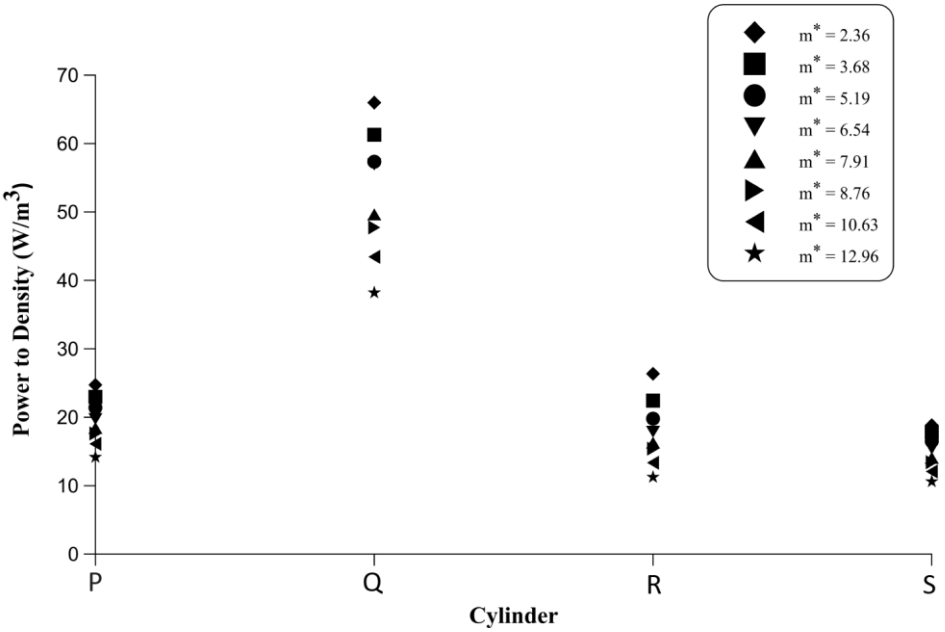

Fig. 11. Maximum Power-to-Volume Density for the four cylinders with different m*

4. Conclusions

The present research used numerical simulation to investigate the influence of m* on the response of VIV in the VIV converter model. Additionally, the research analyzed the energy conversion aspect of the studied model. Furthermore, the study attempted to examine the variance in power-to-volume density for VIVACE power production at varied m*, an area that has received minimal previous investigation. In order to accomplish this objective, the research conducted a comprehensive examination of eight m*, namely 2.36, 3.68, 5.19, 6.54, 7.91, 8.76, 10.63, and 12.96, which were used as constituents for the four cylinders.

The investigation emphasizes considerable attention to the variation in m* while exploring the varied properties of vortices. In order to get a comprehensive comprehension of the VIV phenomena and increase power production, it is crucial to conduct more studies. Further research is necessary to determine the critical elements that influence VIV and fabricate suitable methods for mitigating diverse m* in order to augment power production. Hence, a number of suggestions are proposed to further investigate the influence of various m* on VIV converters, which are necessary for the transformation of environmentally friendly energy into electrical power.

To significantly increase the average power-to-volume density, it is advisable to decrease the m* and increase the reduced velocity for the four cylinders. The current study demonstrates that the maximum average power-to-volume density obtained is 290 W/m^3 when the value of m* is equal to 2.36. In essence, reducing the m* while sustaining an elevated decreased velocity raises the average power-to-volume density. This improvement guarantees an ample power supply to cater to the demands of the offshore sector.

Acknowledgment
This research was funded by the Ministry of Higher Education of Malaysia (Award No. FRGS/1/2022/TK06/UMT/02/7, Vot No. 59713).

References

[1] Chirathalattu, Abraham Thomas, B. Santhosh, Chandan Bose, Rony Philip, and Bipin Balaram. "Passive suppression of vortex-induced vibrations using a nonlinear energy sink-Numerical and analytical perspective." *Mechanical Systems and Signal Processing* 182 (2023): 109556. https://doi.org/10.1016/j.ymssp.2022.109556

[2] Sarpkaya, Turgut. "A critical review of the intrinsic nature of vortex-induced vibrations." *Journal of Fluids and Structures* 19, no. 4 (2004): 389-447. https://doi.org/10.1016/S0889-9746(04)00035-0

[3] Gonçalves, Rodolfo T., Guilherme F. Rosetti, André LC Fujarra, and Allan C. Oliveira. "Experimental study on vortex-induced motions of a semi-submersible platform with four square columns, Part I: Effects of current incidence angle and hull appendages." *Ocean Engineering* 54 (2012): 150-169. https://doi.org/10.1016/j.oceaneng.2012.06.032

[4] Han, Peng, Qiaogao Huang, Guang Pan, Wei Wang, Tianqi Zhang, and Denghui Qin. "Energy harvesting from flow-induced vibration of a low-mass square cylinder with different incidence angles." *AIP Advances* 11, no. 2 (2021). https://doi.org/10.1063/5.0037071

[5] Kotoa, Jaswar, and Abdul Khair Junaidia. "Analysis of Vortex-Induced Vibration of Riser using Spalart-Almaras Model." *Jurnal Teknologi* 69, no. 7 (2014): 69. https://doi.org/10.11113/jt.v69.3260

[6] Wang, Wei, and Fuwang Zhao. "Numerical investigation on flow-induced vibration response of the cylinder inspired by the honeycomb." *Ocean Engineering* 268 (2023): 113461. https://doi.org/10.1016/j.oceaneng.2022.113461

[7] Williamson, C. H. K., and R. Govardhan. "A brief review of recent results in vortex-induced vibrations." *Journal of Wind Engineering and Industrial Aerodynamics* 96, no. 6-7 (2008): 713-735. https://doi.org/10.1016/j.jweia.2007.06.019

[8] Rahman, Mohd Asamudin A., Fatin Alias, and Mohd Hairil Mohd. "Flow Past of a Drilling Riser System with Auxiliary Lines in Laminar Flow." *CFD Letters* 15, no. 2 (2023): 101-113. https://doi.org/10.37934/cfdl.15.2.101113

[9] Alias, Fatin, Mohd Hairil Mohd, Mohd Azlan Musa, Erwan Hafizi Kasiman, and Mohd Asamudin A. Rahman. "Flow Past a Fixed and Freely Vibrating Drilling Riser System with Auxiliaries in Laminar Flow." *Journal of Advanced Research in Fluid Mechanics and Thermal Sciences* 87, no. 3 (2021): 94-104.

[10] Min, Yaobing, Wenchang Wu, Hongda Zhang, and Xingsi Han. "Self-adaptive turbulence eddy simulation of flow control for drag reduction around a square cylinder with an upstream rod." *European Journal of Mechanics-B/Fluids* 100 (2023): 185-201. https://doi.org/10.1016/j.euromechflu.2023.03.008

[11] Silva-Ortega, M., and Gustavo Roque da Silva Assi. "Hydrodynamic loads on a circular cylinder surrounded by two, four and eight wake-control cylinders." *Ocean Engineering* 153 (2018): 345-352. https://doi.org/10.1016/j.oceaneng.2018.01.116

[12] Behrouzi, Fatemeh, Mehdi Nakisa, Adi Maimun, and Yasser M. Ahmed. "Renewable energy potential in Malaysia: Hydrokinetic river/marine technology." *Renewable and Sustainable Energy Reviews* 62 (2016): 1270-1281. https://doi.org/10.1016/j.rser.2016.05.020

[13] Bernitsas, Michael M., Kamaldev Raghavan, Y. Ben-Simon, and E. M. H. Garcia. "VIVACE (vortex induced vibration aquatic clean energy): a new concept in generation of clean and renewable energy from fluid flow." In *International Conference on Offshore Mechanics and Arctic Engineering*, vol. 47470, pp. 619-637. 2006. https://doi.org/10.1115/OMAE2006-92645

[14] Bernitsas, Michael M., Y. Ben-Simon, Kamaldev Raghavan, and E. M. H. Garcia. "The VIVACE converter: model tests at high damping and reynolds number around 10 5." *Journal of Offshore Mechanics and Arctic Engineering* 131, no. 1 (2009): 011102. https://doi.org/10.1115/1.2979796

[15] Zhang, Baoshou, Baowei Song, Zhaoyong Mao, Wenlong Tian, and Boyang Li. "Numerical investigation on VIV energy harvesting of bluff bodies with different cross sections in tandem arrangement." *Energy* 133 (2017): 723-736. https://doi.org/10.1016/j.energy.2017.05.051

[16] Fredsoe, Jorgen, and B. Mutlu Sumer. *Hydrodynamics around cylindrical structures*. Vol. 12. World Scientific, 1997. https://doi.org/10.1006/jfls.1997.0117

[17] Reyes, Mandujano, and F. Mandujano. "Vortex induced vibrations of a cylinder at low mass ratio." *European Journal of Mechanics-B/Fluids* 91 (2022): 66-79. https://doi.org/10.1016/j.euromechflu.2021.09.012

[18] Gonçalves, Rodolfo Trentin, Guilherme Feitosa Rosetti, Guilherme Rosa Franzini, Julio Romano Meneghini, and André Luís Condino Fujarra. "Two-degree-of-freedom vortex-induced vibration of circular cylinders with very low aspect ratio and small mass ratio." *Journal of Fluids and Structures* 39 (2013): 237-257. https://doi.org/10.1016/j.jfluidstructs.2013.02.004

[19] Liu, Mingming, Ruijia Jin, and Haocheng Wang. "Numerical investigation of vortex induced vibration of a circular cylinder for mass ratio less than 1.0." *Ocean Engineering* 251 (2022): 111130. https://doi.org/10.1016/j.oceaneng.2022.111130

[20] Zahari, M. A., and S. S. Dol. "Application of vortex induced vibration energy generation technologies to the offshore oil and gas platform: The preliminary study." *International Journal of Aerospace and Mechanical Engineering* 8, no.

7 (2014): 1321-1324.
[21] Rahman, Mohd Asamudin A., Jeremy Leggoe, Krish Thiagarajan, Mohd Hairil Mohd, and Jeom Kee Paik. "Numerical simulations of vortex-induced vibrations on vertical cylindrical structure with different aspect ratios." *Ships and Offshore Structures* 11, no. 4 (2016): 405-423. https://doi.org/10.1080/17445302.2015.1013783
[22] Wang, Yupu, Wenming Cheng, Run Du, Shubiao Wang, and Yong Deng. "Numerical investigation of flow around two tandem identical trapezoidal cylinders." *Mathematical Problems in Engineering* 2020 (2020): 1-13. https://doi.org/10.1155/2020/3759834
[23] Fredsoe, Jorgen, and Rolf Deigaard. *Mechanics of coastal sediment transport*. Vol. 3. World Scientific Publishing Company, 1992.
[24] Mishra, Rahul, Atul Soti, Rajneesh Bhardwaj, Salil S. Kulkarni, and Mark C. Thompson. "Transverse vortex-induced vibration of a circular cylinder on a viscoelastic support at low Reynolds number." *Journal of Fluids and Structures* 95 (2020): 102997. https://doi.org/10.1016/j.jfluidstructs.2020.102997
[25] Zhang, Baoshou, Zhaoyong Mao, Baowei Song, Wenlong Tian, and Wenjun Ding. "Numerical investigation on VIV energy harvesting of four cylinders in close staggered formation." *Ocean Engineering* 165 (2018): 55-68. https://doi.org/10.1016/j.oceaneng.2018.07.042
[26] Derakhshandeh, J. F., and Md Mahbub Alam. "A review of bluff body wakes." *Ocean Engineering* 182 (2019): 475-488. https://doi.org/10.1016/j.oceaneng.2019.04.093
[27] Xu, Liang-bin, Sheng-ping Liang, Zhong-ming Hu, Zheng-li Liu, and Jia-song Wang. "Vortex-induced vibration response of a circular cylinder surrounded with small rods." *Journal of Hydrodynamics* 33, no. 3 (2021): 510-519. https://doi.org/10.1007/s42241-021-0045-5
[28] Desai, Aditya, Sanchit Mittal, and Sanjay Mittal. "Experimental investigation of vortex shedding past a circular cylinder in the high subcritical regime." *Physics of Fluids* 32, no. 1 (2020). https://doi.org/10.1063/1.5124168
[29] Kang, Zhuang, Cheng Zhang, Rui Chang, and Gang Ma. "A numerical investigation of the effects of Reynolds number on vortex-induced vibration of the cylinders with different mass ratios and frequency ratios." *International Journal of Naval Architecture and Ocean Engineering* 11, no. 2 (2019): 835-850. https://doi.org/10.1016/j.ijnaoe.2019.02.012